

Phase-Coherent Temperature Amplifier

Federico Paolucci,^{*,†} Giampiero Marchegiani,^{†,‡} Elia Strambini,[†] and Francesco Giazotto[†]

NEST, Istituto Nanoscienze-CNR and Scuola Normale Superiore, I-56127 Pisa, Italy

E-mail: federico.paolucci@nano.cnr.it

Abstract

Coherent caloritronics, the thermal counterpart of coherent electronics, has drawn growing attention since the discovery of heat interference in 2012. Thermal interferometers, diodes, transistors and nano-valves have been theoretically proposed and experimentally demonstrated by exploiting the quantum phase difference between two superconductors coupled through a Josephson junction. So far, the quantum-phase modulator has been realized in the form of a superconducting quantum interference device (SQUID) or a superconducting quantum interference proximity transistor (SQUIPT). Thence, an external magnetic field is necessary in order to manipulate the heat transport. Here, we theoretically propose the first on-chip fully thermal caloritronic device: the phase-coherent temperature amplifier. Taking advantage of a recent thermoelectric effect discovered in spin-split superconductors coupled to a spin-polarized system, by a temperature gradient we generate the magnetic flux controlling the transport through a temperature biased SQUIPT. By employing commonly used materials and a geometry compatible with state-of-the-art nano-fabrication techniques, we simulate the behavior of the temperature amplifier and define a number of figures of merit in full analogy with voltage amplifiers. Notably, our architecture ensures infinite input thermal impedance, maximum gain of about 11 and efficiency reaching the 95%. This device concept could represent a breakthrough in coherent caloritronic devices, and paves the way for applications in radiation sensing, thermal logics and quantum information.

Introduction

The discovery of thermoionic emission by Fredrick Guthrie in 1873¹ brought to the invention of the first electronic devices: the diode and triode amplifier.² These pioneering works paved

the way to the development of electronic apparatuses as well as radio, television and telephone. After more than 100 years, the recent advances of transistor-based technology³ made possible the design and production of new daily life devices as computers, tablets and smartphones. In the era of energy saving, the common goal in electronics is to increase the device efficiency in order to abate energy losses and pollutant emissions. Anyways, further developments of nowadays technology are

^{*}To whom correspondence should be addressed

[†]NEST, Istituto Nanoscienze-CNR and Scuola Normale Superiore, I-56127 Pisa, Italy

[‡]Dipartimento di Fisica dell'Università di Pisa, Largo Pontecorvo 3, I-56127 Pisa, Italy

bounded by quantum mechanical restrictions to miniaturization and by heat dissipation.⁴ Despite it is considered detrimental in electronics, the ability of mastering the transport of the inescapable heat generated in solid-state nano-structures has been only recently investigated,⁵ and it could lead to new device concepts and capabilities. In this framework, the experimental demonstration in 2012 of heat interference in a superconducting quantum interference device (SQUID)⁶ heralded the foundation of the thermal counterpart of coherent electronics: the coherent caloritronics.^{7,8} Despite it is still distant from the ripeness of electronics, coherent caloritronics is rapidly growing through the design and the realization of thermal analogues of electronic devices, such as heat diodes,^{6,9,10} transistors,¹¹ valves,¹² amplifiers¹³ and modulators.^{14,15} One of the theoretical foundations of coherent caloritronics resides in the prediction of the periodic dependence of thermal currents across a Josephson junction¹⁶ on the quantum phase difference between the two superconductors.¹⁷ As a consequence, the thermal modulation in such systems acquires a phase-coherent character.

So far, the quantum interference mechanism between Josephson-coupled superconductors has been experimentally realized through the use of a SQUID¹⁸ or, more recently, taking advantage from a newly designed superconducting quantum interference proximity transistor (SQUIPT).^{19–21} Thereby, the thermal transport across caloritronic devices is manipulated by a magnetic flux Φ threading a superconducting ring, and an external source of magnetic field is essential. The last requirement impeded the realization of fully thermal on-chip coherent caloritronic devices up to now. In the last two years, surprisingly large thermoelectric effects in spin-filtered superconducting tunnel junctions have been theoretically predicted²⁴ and experimentally demonstrated.²⁶ This discovery enables the direct transduction, for the first time at cryogenic temperatures, of temperature gradients into electrical signals with unprecedented efficiency.

Here, we present the first on-chip fully thermal device in caloritronics: the phase-coherent temperature amplifier. Our architecture takes advantage from the closed-circuit current generated by a

thermoelectric element in order to create a magnetic field, through the simple Biot-Savart law, which controls heat transport across a thermal nano-valve. By employing experimentally widely used materials and a geometry feasible with standard lithographic techniques, we show the basic input-to-output temperature conversion, and define several figures of merit in analogy to electronics to evaluate the performances of the temperature amplifier. The device layout may foster its use in different field of science, as well as quantum information,^{27,28} thermal logics²⁹ and ultrasensitive radiation detection.⁵

Results and discussion

The phase-coherent temperature amplifier is the caloritronic equivalent of the voltage amplifier in electronics.^{30,31} In fact, temperature is the thermal counterpart of electric potential. On the other hand, the thermal current can not be analogized to the electrical current, because physically it is a thermal power flow. Therefore, the thermal current amplifier results to be the counterpart of the power amplifier in electronics. The voltage-temperature analogy is schematized in Figure 1-a, where the usual symbol of voltage amplifiers (blue) and the corresponding representation of temperature amplifiers (red) are depicted. A voltage amplifier is a device which produces an output signal $V_{OUT} = G \Delta V_{IN}$, where $G > 1$ is the gain and $\Delta V_{IN} = V_{IN} - V_{REF}$ is the difference between the input signal V_{IN} and the reference V_{REF} . Since the law of conservation of energy does not allow the creation of energy, the system requires a voltage supply V_S to operate. Analogously, a temperature amplifier generates an output temperature $T_{OUT} = G T_{IN}$, where T_{IN} is the input signal. In this case, the operation power is supplied by a temperature T_S . Differently from electronics, where the absolute value of the signals has no physical meaning and an arbitrary reference potential is required, in caloritronics the temperature signals can take only positive values and they are always referred to zero temperature (which represents zero energy). Thereby, the base temperature T_{BATH} has a different and more complex role than a simple reference. It defines the background energy level, the operation¹² and

the energy losses of the system due to electron-phonon interaction.⁵ In the following, we set a value of the reference temperature achievable with standard dilution refrigerators $T_{BATH} = 10$ mK that ensures low noise and reduced energy losses.

The phase-coherent temperature amplifier is composed of a normal metal-ferromagnetic insulator-superconductor ($N-FI-S$) tunnel junction inductively coupled to a SQUIPT¹⁹ through a superconducting coil, as sketched in Figure 1-b. The working principle of such a device is rather simple: a temperature gradient across the $N-FI-S$ junction induces the flow of an electronic current into the superconducting coil which provides a magnetic flux threading the SQUIPT. This controls the thermal transport across the latter. Since the two building blocks (the $N-FI-S$ junction and the SQUIPT) have been only recently proposed, we start describing their behavior separately and we couple them successively.

In an electronic conductor, thermoelectricity can be generated by breaking the electron-hole symmetry in the density of states (DOS).²² In a superconductor, this condition can be accomplished by Zeeman spin-splitting the DOS through an exchange field h_{ex} and spin-filtering the quasiparticles.^{23,24} In our scheme, both the mechanisms are provided by a single ferromagnetic insulator layer of the $N-FI-S$ junction,³² highlighted with the dashed rectangle in Figure 1-b. A temperature gradient between the normal metal N (yellow block) and the superconductor S (turquoise block) generates the thermoelectric signal: an open circuit thermovoltage V_T in the Seebeck regime or a closed circuit thermocurrent I_T in the Peltier regime.³² In our device, we take advantage of the closed circuit thermocurrent in order to create a magnetic field by means of a dissipationless superconducting coil of self-inductance L . The superconductor is kept at T_{BATH} while the normal metal is set to the input temperature $T_{IN} > T_{BATH}$, because in this configuration the provided thermocurrent exhibits a monotonic behavior with rising temperature gradient (see Figure 1-c).³² The detailed description of the temperature-to-current transduction of the $N-FI-S$ junction can be found in the Methods. Figure 1-c shows the dependence of the closed circuit current I_T on the temperature of the normal metal T_{IN} for different values of the exchange field

h_{ex} . The thermocurrent is a growing function of the spin-splitting of the DOS (i.e. h_{ex}) and abruptly increases for $T_{IN} \geq 200$ mK. As a consequence, the magnetic flux created by the coil will monotonically strengthen with the input temperature T_{IN} .

We now turn our attention on the second building block of our device: the thermally biased SQUIPT. It is composed of a normal metal wire N_1 interrupting a superconducting ring S_1 (red ring), as portrayed in Figure 1-b. Owing to the good electric contact between S_1 and N_1 , the metal wire acquires a superconducting character through the so-called superconducting proximity effect.²⁵ A normal metal N_2 probe (orange block) is tunnel-coupled to the wire through a thin insulating layer and acts as the output electrode of the temperature amplifier. A magnetic flux Φ threading the ring modulates the density of states of the proximized wire and, as a consequence, the electronic transport between N_1 and the normal metal probe.¹⁹⁻²¹ Analogously, temperature-biased SQUIPT has been predicted to act as a thermal nano-valve leading to a phase-dependent thermal transport between the superconducting ring and the tunnel probe.¹² The detailed theoretical description of the SQUIPT can be found in the Methods. The thermal behavior of the nano-valve is resumed in Figure 1-d, where the dependence of the probe temperature T_{OUT} on the magnetic flux Φ for different values of the ring temperature T_S is plotted. The probe temperature is minimum at $\Phi = 0$, reaches its maximum at $\Phi \sim 0.45 \Phi_0$ and lowers for $\Phi \rightarrow \Phi_0/2$. Accordingly, the same behavior characterizes the thermal conductance and the flux-to-temperature transfer function.¹² Furthermore, the maximum value of T_{OUT} increases with T_S while its modulation with the magnetic flux softens for large values of the S_1N_1 ring temperature. Notably, thermal transport across the SQUIPT is fully phase-coherent, because it is modulated by the superconducting macroscopic phase difference across the proximized wire.¹² Essentially, the magnetic flux strives to close the induced energy gap in the wire, and the latter tends to a metallic character,¹⁹ accordingly.

The architecture of the temperature amplifier requires to couple the two building blocks. This goal is achieved by means of the superconducting coil of inductance L (see Figure 1-b). Notably,

our vertical concentric geometry does not impose constraints to the inductance of the second block (i.e. the SQUIPT), because the thermal nano-valve is placed at the center of the coil which is supposed to have the same diameter as the SQUIPT loop and, as a consequence, all the magnetic flux generated by the coil will thread the superconducting ring. Therefore, the magnetic flux through the SQUIPT is $\Phi = L I_T$.

This assembly permits to relate the input T_{IN} with the output T_{OUT} temperature. In analogy with voltage amplifiers, we define the temperature sensitivity $Sens$ as the input signal $T_{IN_{MAX}}$ necessary to produce the maximum possible output $T_{OUT_{MAX}}$. Since the maximum transmissivity of the SQUIPT is reached at $\Phi \sim 0.45 \Phi_0$ (as illustrated in Figure 1-d), the coupling inductance is determined by the expression $L = 0.45 \Phi_0 / I_{T_{MAX}}$, where $I_{T_{MAX}}$ is the current generated by the thermoelectric element at input temperature $T_{IN} = Sens$. Through this definition, the output is a growing function of the input signal, as normally required to an amplifier. Thence, we can associate all values of the input signal that abide by $T_{IN} \leq Sens$ with the resulting output temperature T_{OUT} . We emphasize that the coupling inductance L scales inversely with increasing temperature sensitivity (i.e. $Sens \sim 1/L$), because the maximum thermocurrent $I_{T_{MAX}}(T_{IN} = Sens)$ rises with the sensitivity (a smaller coupling L is necessary in order to generate a flux $\Phi(T_{IN} = Sens) = 0.45 \Phi_0$ for higher values of $Sens$).

In the following, we will simulate the behavior of the temperature amplifier and define a number of figures of merit in analogy to conventional voltage amplifiers. These calculations will be performed by employing realistic materials and feasible geometry, as extensively described in the Methods.

The basic behavior of the temperature amplifier is illustrated in Figure 2-a, where the dependence of the output temperature T_{OUT} on the input temperature T_{IN} is depicted for a supply temperature $T_S = 250$ mK and for different sensitivities $Sens$. The horizontal dotted black line represents the minimum value of the output active range OAR (i.e. the interval where the output varies with the input signal) defined as $T_{OUT_{MIN}} = T_{Noise} + 10\% T_{Noise}$, where the noise temperature

$T_{Noise} = T_{OUT}(T_{IN} = T_{BATH})$ is the output temperature for a null input signal (i.e. when the normal layer N is at the temperature of the bath). Both the maximum value of the output signal $T_{OUT_{MAX}}$ and the noise level T_{Noise} do not depend on the choice of the sensitivity $Sens$, because the thermal conductivity of the SQUIPT at $\Phi = 0$ and $\Phi = 0.45 \Phi_0$ is only a function of the supply temperature T_S ,¹² as elucidated in the Methods. Thereby, the device is characterized by a constant output active range $OAR = T_{OUT_{MAX}} - T_{Noise} \sim 130$ mK, as depicted in Figure 2-a. On the other hand, T_{OUT} calculated at a specific T_{IN} drops by increasing $Sens$, because at a fixed T_{IN} the thermocurrent is independent of the sensitivity, and the inducing coupling constant L lowers by increasing $Sens$.

The density of states of the proximized wire N_{wire} is composed of a phase-dependent and a phase-independent component,¹⁹ as mathematically expounded by Equation ?? of the Methods. The balance of the two parts defines the thermal transport through the SQUIPT. For instance, the supply temperature T_S has a great influence on the behavior of the phase-coherent temperature amplifier, because it defines the minimum and the maximum values of the output signal T_{OUT} , as illustrated in Figure 2-b in the case of $Sens = 50$ mK. For values of T_S comparable to the critical temperature T_{C-S_1} of the ring of the SQUIPT, T_{OUT} weakly depends on T_{IN} , because the energy gap of the ring Δ_{S_1} closes and the proximized wire assumes an almost metallic character for every value of the magnetic flux Φ (i.e input temperature T_{IN}). By lowering T_S the superconducting pairing potential rises. As a consequence, the phase-dependent and the phase-independent parts of proximized DOS of the wire N_{wire} become comparable (see the Methods), the flux Φ successfully modulates thermal transport across the SQUIPT in the complete range $0 - 0.45 \Phi_0$, and the output temperature varies with all the values of the input signal (see the traces for $T_S = 450 - 150$ mK in Figure 2-b). When $T_S \leq 0.1 T_{C-S_1}$ the energy gap of the ring acquires almost its zero temperature value ($\Delta_{S_1} \approx \Delta_{0-S_1}$), and the phase-dependent part of the thermal transport becomes dominant only when $\Phi \rightarrow 0.45 \Phi_0$. Thereby, the output temperature is exclusively modulated for $T_{IN} \approx Sens$ and the output signal can be lower than the input, as shown

for $T_S = 60$ mK in Figure 2-b, where the gray rectangle represents the region with $T_{IN} \geq T_{OUT}$. The ensemble of these behaviors leads to the conclusion that the temperature amplifier efficiently works when $0.1 T_{C-S_1} \leq T_S \leq 0.4 T_{C-S_1}$.

The most relevant parameter for an amplifier is the gain G , which is plotted in Figure 2-c as a function of the input temperature for different values of $Sens$ and $T_S = 250$ mK. The gain is constant over different values of sensitivity in the case of $T_{IN} = T_{BATH}$, because the noise level T_{Noise} is only determined by T_S . On the other hand, G strongly depends on $Sens$ when the output temperature resides in the OAR (i.e. $T_{OUT} \geq T_{OUT_{MIN}}$). In particular, G lowers by increasing sensitivity at fixed T_{IN} , and $G(T_{IN} = Sens)$ drops for rising $Sens$, because the coupling inductance scales inversely with the sensitivity and the maximum output signal is exclusively controlled by the supply temperature (see Figure 2-a). For a given $Sens$, the gain grows with T_{IN} when the amplifier is in the active output mode, i.e. the values of G above the black dotted line in Figure 2-c. This behavior is the result of the joint action of the temperature-to-current conversion due to the thermoelectric element and the dependence of the thermal transport across the SQUIPT on the magnetic flux through it (a comprehensive explanation can be found in the Methods).

Depending on the requirements, one can opt for low values of T_S in order to increase the active output range or choose high values of supply temperature to maximize the gain. Since the behavior of the device is satisfactory both in terms of gain and output active range only in a limited range of supply temperatures, increasing the critical temperature of the ring of the SQUIPT could be beneficial in terms of device performances. Higher values of T_{C-S_1} would guarantee wider OAR and larger G at $T_{IN} = Sens$. The maximum value of the gain in the active region at the optimal constant ratio $T_{C-S_1}/T_S \approx 5.2$ rises linearly with the critical temperature of the SQUIPT for every value of sensitivity, as depicted in Figure 2-d. We employ aluminum as S_1 , because the feasibility of Al-based SQUIPTs has been already demonstrated,^{19,33} but there are no fundamental theoretical reasons, in principle, to avoid the use of such materials. Therefore, the phase-coherent temper-

ature amplifier could potentially be used both at higher values of T_S and T_{IN} ensuring large G and wide OAR too.

In full analogy with electronics, we define particular figures of merit for the temperature amplifier, i.e. numerical parameters that characterize its properties and performances. First of all, the input impedance is a fundamental parameter in voltage amplifiers. In electronics, a voltage amplifier is considered ideal when the input impedance is infinite and, as a consequence, the load of the input and output circuits are completely decoupled. We wish to point out that the input thermal impedance Z_{IN}^{th} of this system is infinite. This arises from the contactless coupling between the input and the output electrodes, as schematized in Figure 1-b. In particular, the double thermal-to-electrical-to-thermal transduction ensures a perfect heat decoupling between the input load and the output signal. Thereby, our device can be classified as an ideal temperature amplifier.

Another important parameter is the input amplification range, IAR , that represents the interval of the input signal for which the output resides in the active range. It is defined as:

$$IAR = Sens - T_{IN}(T_{OUT_{MIN}}), \quad (1)$$

where $T_{IN}(T_{OUT_{MIN}})$ is the value of the input temperature corresponding to the minimum value of the output active range. The IAR is a function both of the supply temperature and of the sensitivity, as illustrated in Figure 3-a. For small values of T_S the active output range is small and, hence, the input amplification range is not extended too. By rising the supply temperature the IAR enlarges till T_S reaches about 250 mK. A further increase of the supply temperature yields a softening of the pairing potential Δ_{S_1} of the SQUIPT, and a consequent compression of OAR , as already elucidated above. The reduction of the output active range is mirrored in a narrowing of the IAR . The non-monotonic behavior of the input amplification range with the sensitivity can be ascribed to the thermoelectric element. On the one hand, the increase of $Sens$ naturally enlarges the IAR by widening the total input temperature range. On the other hand, the closed circuit thermocurrent rapidly rises with T_{IN} , as illustrated in Figure 1-c.

The resulting magnetic flux Φ is modulated only for values of the input temperature approaching $Sens$, because the coupling constant L is small and for the thermocurrents typical of narrow temperature gradients the flux always tends to zero. The latter effect manifests itself in lowering IAR for increasing $Sens$, as shown in Figure 3-a.

In the era of energy saving, a great focus concerns the device efficiency η . In electronics it is defined as the ratio between the maximum output signal and the supply necessary to power the device. For a temperature amplifier η takes the form:

$$\eta = \frac{T_{OUT_{MAX}}}{T_S} \times 100, \quad (2)$$

where $T_{OUT_{MAX}} = T_{OUT}(T_{IN} = Sens)$ (i.e. the output signal when the input temperature acquires the value of the sensitivity). The efficiency reaches $\sim 95\%$ for very small supply temperatures and monotonically decreases with rising T_S , as plotted in Figure 3-b. The drop of η can be explained with the closure of the gap of the SQUIPT Δ_{S_1} (as already explained above) and the growth of the losses through the phonons resulting from the temperature increase.⁵ In the region of best performances in terms of OAR , G and IAR (represented with the yellow rectangle in Figure 3-b) the efficiency ranges from $\sim 90\%$ to $\sim 60\%$. These large η values are comparable to analogous commercial electronic amplifiers.

The output active range provides a first and reliable estimate of the useful interval of the output signal. A more complete analysis requires to define and employ the output dynamic range DR , which is defined:

$$DR = 20 \times \log \left(\frac{T_{OUT_{MAX}} + T_{Noise}}{T_{Noise}} \right). \quad (3)$$

The output dynamic range widens by increasing supply temperature up to $T_S = 150$ mK, because $T_{OUT_{MAX}}$ rises while T_{Noise} is almost unaffected (as shown in the inset of Figure 3-c). Further increase of T_S enlarges the noise with a steeper rate, while $T_{OUT_{MAX}}$ tends to level to a constant value. As a consequence, DR decreases for values of T_S approaching the SQUIPT critical temperature. Despite that, the phase-coherent temperature amplifier reaches the maximum performances in terms

of DR in occurrence of the figures of merit we have already defined above, as depicted by the turquoise rectangle in Figure 3-c.

Furthermore, we consider the differential gain DG , defined as:

$$DG = \frac{dT_{OUT}}{dT_{IN}}. \quad (4)$$

At a fixed sensitivity, DG displays a bell-like shape, as shown in Figure 3-d. The height, width and position of the peak are sensitivity-dependent. In particular, for small and large values of $Sens$ the peak is high and narrow, while for intermediate sensitivities the peak is low and broad in T_{IN} . This behavior can be foreseen by carefully looking to Figure 2-a, where the direct dependence of T_{OUT} with T_{IN} is revealed. Since DG is always greater than zero, the output signal is always a monotonically growing function of the input, as required for an amplifier. Unfortunately, the non-linear nature of the building blocks constituting the temperature amplifier causes a non-linear gain resulting in a distortion of the output signal.

Finally, the phase-coherent temperature amplifier ensures thermal power damping. The latter is direct consequence of the device architecture. In particular, the nature of the tunnel junctions typical of the thermoelectric element and the SQUIPT (see the Methods) abates the thermal power along the device. Thereby, the temperature amplifier can be implemented in on-chip hybrid caloritronic/electronic devices, because it is able to process a temperature signal while decreasing the heat power detrimental for solid-state electronic nano-structures.

Conclusions

In summary, we have proposed and theoretically investigated the phase-coherent temperature amplifier, which is the caloritronic counterpart of the voltage amplifier in electronics. The pivotal architecture proposed in this work constitutes the first fully-thermal on-chip device in coherent caloritronics, because the magnetic field necessary to control the thermal nano-valve (i.e. the SQUIPT) is self-generated by the use of a thermoelectric element (a $N - FI - S$ junction). The op-

erating principle and the performances have been studied in detail paying specific attention to the experimental feasibility of geometry and material composition. The predicted input-to-output temperature conversion provides a maximum gain $G \approx 11$ at small input signals which is mainly limited by the superconducting critical temperature T_{C-S_1} of the aluminum-based nano-valve. In addition, we defined several figures of merit in full

analogy with voltage amplifiers obtaining remarkable results especially in terms of output dynamic range DR and efficiency η . Finally, we point out that this phase-coherent device can pave the way to new opportunities in research fields where mastering thermal transport between different bodies is fundamental, as well as in quantum computing, thermal logics and ultra-sensitive single-photon sensing.

Methods

N-FI-S junction

The thermoelectric element is composed of a tunnel junction made of a normal metal N at temperature T_{IN} , a ferromagnetic insulator FI and a superconductor S kept at T_{BATH} . The FI layer operates a double action: it behaves as a spin filter with polarization $P = (G_{\uparrow} - G_{\downarrow}) / (G_{\uparrow} + G_{\downarrow})$ where G_{\uparrow} and G_{\downarrow} are the spin up and spin down conductances,³⁴ and it causes the spin-splitting of the DOS of the superconductor by the interaction of its localized magnetic moments with the conducting quasiparticles in S through an exchange field h_{ex} . Since the exchange interaction in a superconductor decays over the coherence length ξ_0 ,³⁵ we assume S thinner than ξ_0 and a spatially homogeneous spin-splitting DOS:²³

$$N_{\uparrow,\downarrow}(E) = \frac{1}{2} \left| \Re \left[\frac{E + i\Gamma \pm h_{ex}}{\sqrt{(E + i\Gamma \pm h_{ex})^2 - \Delta^2}} \right] \right|, \quad (5)$$

where E is the energy, Γ is the Dynes parameter accounting for broadening,³⁶ and $\Delta(T_{BATH}, h_{ex})$ is the temperature and exchange field-dependent superconducting energy gap. The pairing potential is calculated self-consistently from the BCS equation:^{23,37}

$$\ln \left(\frac{\Delta_0}{\Delta} \right) = \int_0^{\hbar\omega_D} \frac{f_+(E) + f_-(E)}{\sqrt{E^2 + \Delta^2}} dE \quad (6)$$

where $f_{\pm}(E) = \left\{ 1 + \exp \left[\left(\sqrt{E^2 + \Delta^2} \mp h_{ex} \right) / k_B T_{BATH} \right] \right\}^{-1}$ is the Fermi distribution of the spin-polarized electrons, ω_D is the Debye frequency of the superconductor, Δ_0 is the zero-field and zero-temperature superconducting gap, and k_B is the Boltzmann constant. The tunnel thermocurrent in the closed circuit configuration (i.e. with the thermoelectric element closed by a superconducting circuit) takes the form:

$$I_T = \frac{1}{eR_T} \int_{-\infty}^{\infty} [N_+(E) + PN_-(E)] [f_N(E, T_{IN}) - f_S(E, T_{BATH})] dE, \quad (7)$$

where e is the electron charge, R_T is the tunnel resistance in the normal state, $N_{\pm}(E) = N_{\uparrow}(E) \pm N_{\downarrow}(E)$, $f_N(E, T_{IN}) = [1 + \exp(E/k_B T_{IN})]^{-1}$ is the Fermi distribution of the metal, and $f_S(E, T_{BATH}) = [1 + \exp(E/k_B T_{BATH})]^{-1}$ is the Fermi function of the superconductor. From the above equation follows that the charge current flowing in the circuit is only due to the temperature gradient and no external voltage bias is needed. Thence, the $N - FI - S$ junction behaves as a thermoelectric element.

Temperature-biased SQUIPT

We model the SQUIPT as a superconducting ring S_1 interrupted by a one-dimensional normal metal wire N_1 ($l \gg w, t$ where l , w and t are the wire length, width and thickness, respectively). The superconducting properties acquired by the wire through the proximity effect²⁵ are modulated by the magnetic flux Φ threading the ring.¹⁹ A normal metal N_2 probe is tunnel-coupled to the wire through a thin insulating layer, and acts as the output electrode.

The DOS of the wire $N_{wire} = |\Re[g^R]|$ is the real part of the quasi-classical retarded Green's function g^{R38} obtained by solving the one-dimensional Usadel equation.³⁹ In the short junction limit (i.e. when $E_{Th} = \hbar D/l^2 \gg \Delta_{S_1}$, where E_{Th} is the Thouless energy, \hbar is the reduced Planck constant and D is the wire diffusion coefficient) the proximity effect is maximized, and the DOS takes the analytical form:¹²

$$N_{wire}(E, \Phi) = \left| \Re \left[\frac{E - iE_{Th}\gamma g_s}{\sqrt{(E - iE_{Th}\gamma g_s)^2 + [E_{Th}\gamma f_s \cos(\frac{\pi\Phi}{\Phi_0})]^2}} \right] \right|. \quad (8)$$

Above, $\gamma = R_{N_1}/R_{S_1N_1}$ is the transmissivity of the S_1N_1 contact (with R_{N_1} denoting the resistance of the normal wire and $R_{S_1N_1}$ the resistance of the S_1N_1 interface), $g_s(E) = \frac{E + i\Gamma_{S_1}}{\sqrt{(E + i\Gamma_{S_1})^2 - \Delta_{S_1}^2}}$ is the coefficient of the phase-independent part of proximized DOS (with Γ_{S_1} Dynes parameter accounting for broadening³⁶ and Δ_{S_1} BCS temperature dependent energy gap³⁷), $f_s(E) = \frac{\Delta_{S_1}}{\sqrt{(E + i\Gamma_{S_1})^2 - \Delta_{S_1}^2}}$ is the coefficient of the phase-coherent part of proximized DOS, and $\Phi_0 = 2.067 \times 10^{-15}$ Wb is the magnetic flux quantum.

The heat current J tunneling from the S_1N_1 ring to the N_2 probe strongly depends on the temperatures of the ring T_S and of the normal electrode T_{OUT} through the highly non-linear expression:

$$J(T_S, T_{OUT}, \Phi) = \frac{2}{e^2 R_{T_1}} \int_0^\infty N_{wire}(E) [f_0(E, T_S) - f_0(E, T_{OUT})] dE \quad (9)$$

where e is the electron charge, R_{T_1} is the normal state tunnel resistance, and $f_0(E, T) = [1 + \exp(E/k_B T)]^{-1}$ is the Fermi distribution of the quasiparticles in the ring for $T = T_S$ and in the probe for $T = T_{OUT}$.

The steady-state temperature of the probe T_{OUT} depends on the thermal current flowing from S_1N_1 to N_2 and on the exchange mechanism occurring in N_2 . Below ~ 1 K the relaxation is prevalently due to electron-phonon coupling⁵ and can be quantified as $J_{e-ph, N_2}(T_{OUT}, T_{BATH}) = \Sigma V (T_{OUT}^n - T_{BATH}^n)$, where Σ is the electron-phonon coupling constant, V is the volume of the probe and the exponent n depends on the disorder of the system. For metals, in the clean limit $n = 5$, while in the dirty limit $n = 4, 6$.^{5,12} Finally, at the steady state by setting a constant temperature of the superconducting ring T_S the output temperature of the nano-valve T_{OUT} can be obtained by solving the following thermal balance equation:

$$-J(T_S, T_{OUT}, \Phi) + J_{e-ph, N_2}(T_{OUT}, T_{BATH}) = 0. \quad (10)$$

Materials and geometry

The thermoelectric element is supposed to be composed of 15 nm of Cu as N , 1 nm of EuS as FI and 3 nm of Al as S . Within this geometry the Al layer has typically a critical temperature $T_C \approx 3$ K, a resulting zero temperature energy gap $\Delta_0 \approx 456 \mu\text{eV}$, and a Dynes parameter $\Gamma = 1 \times 10^{-4} \Delta_0$. We consider an EuS layer characterized by a polarization $P = 0.95$, an exchange field $h_{ex} = 0.45 \Delta_0$, and a tunnel resistance $R_T = 0.1 \Omega$. The superconducting coil originating the magnetic flux is made of 30 nm thick aluminum

and it is embedded in 40 nm of Al_2O_3 to ensure electrical insulation to the thermal nano-valve. The SQUIPT is supposed to be made of a copper N_1 wire of length $l = 100$ nm, width $w = 30$ nm, thickness $t = 30$ nm and diffusivity $D = 1 \times 10^{-2} \text{ m}^2/\text{s}$, and of a 150 nm thick Al S_1 ring of diameter $d = 1 \mu\text{m}$ with $\Delta_{0-S_1} = 200 \mu\text{eV}$, $T_{C-S_1} \approx 1.32$ K and $\Gamma_{S_1} = 1 \times 10^{-4} \Delta_{0-S_1}$. The transmissivity of the $S_1 N_1$ contact is assumed to be $\gamma = 33$. The AlMn probe is tunnel-coupled to the proximized wire through a 1 nm thick aluminum oxide layer of resistance $R_{T_1} = 100 \text{ k}\Omega$. The parameters of the AlMn electrode are: electron-phonon coupling constant $\Sigma = 4 \times 10^9 \text{ WK}^{-6} \text{ m}^{-3}$,¹¹ volume $V = 1 \times 10^{-20} \text{ m}^3$ and temperature exponent $n = 6$.^{5,9,11}

Acknowledgement The authors acknowledge the European Research Council under the European Unions Seventh Framework Programme (FP7/2007-2013)/ERC Grant No. 615187 - CO-MANCHE and the MIUR under the FIRB2013 Grant No. RBFR1379UX - Coca for partial financial support. The work of E.S. is funded by a Marie Curie Individual Fellowship (MSCA-IFEF-ST No. 660532-SuperMag).

References

1. F. Guthrie, Magnetism and Electricity, *London and Glasgow: William Collins, Sons, & Company*, 1876.
2. M. Guarnieri, The age of vacuum tubes: Early devices and the rise of radio communications, *IEEE Ind. Electron. M.* **2012**, 6, 41-43.
3. E. W. Pugh, L. R. Johnson, and J. H. Palmer, IBM's 360 and early 370 systems, *MIT Press*, Boston, 34.
4. J. Mannhart, and D. G. Schlom, Oxide Interfaces - An Opportunity for Electronics, *Science* **2010**, 327, 1607-1611.
5. F. Giazotto, T. T. Heikkilä, A. Luukanen, A. M. Savin, and J. P. Pekola, Opportunities for mesoscopics in thermometry and refrigeration: Physics and applications, *Rev. Mod. Phys.* **2006**, 78, 217-274.
6. F. Giazotto, and M. J. Martinez-Pérez, The Josephson heat interferometer, *Nature* **2012**, 492, 401-405.
7. M. J. Martinez-Pérez, P. Solinas, and F. Giazotto, Coherent Caloritronics in Josephson-Based Nanocircuits, *J Low Temp Phys* **2014**, 175, 813-837.
8. M. J. Martinez-Pérez, P. Solinas, and F. Giazotto, A quantum diffractor for thermal flux, *Nature Commun.* **2014**, 5, 3579.
9. M. J. Martinez-Pérez, A. Fornieri, and F. Giazotto, Rectification of electronic heat current by a hybrid thermal diode, *Nat. Nanotech.* **2015**, 10, 303-307.
10. M. J. Martinez-Pérez, and F. Giazotto, Efficient phase-tunable Josephson thermal rectifier, *Appl. Phys. Lett.* **2013**, 102, 182602.
11. A. Fornieri, C. Blanc, R. Bosisio, S. D'Ambrosio, and F. Giazotto, Nanoscale phase engineering of thermal transport with a Josephson heat modulator, *Nat. Nanotech.* **2015**, 11, 258-263.
12. E. Strambini, F. S. Bergeret, and F. Giazotto, Proximity nanovalve with large phase-tunable thermal conductance, *Appl. Phys. Lett.* **2014**, 105, 082601.
13. A. Fornieri, G. Timossi, R. Bosisio, P. Solinas, and F. Giazotto, Negative differential thermal conductance and heat amplification in superconducting hybrid devices, *Phys. Rev. B* **2016**, 93, 134508.
14. F. Giazotto, and M. J. Martinez-Pérez, Phase-controlled superconducting heat-flux quantum modulator, *Appl. Phys. Lett.* **2012**, 101, 102601.
15. M. J. Martinez-Pérez, and F. Giazotto, Fully balanced heat interferometer, *Appl. Phys. Lett.* **2013**, 102, 092602.
16. B. D. Josephson, Possible new effects in superconductive tunneling, *Phys. Lett.* **1962**, 1, 251-253.

17. K. Maki, and A. Griffin, Entropy transport between two superconductors by electron tunneling, *Phys. Rev. Lett.* **1965**, 15, 921-923.
18. J. Clarke, and A. I. Braginski, eds. The SQUID Handbook, *Wiley-VCH*, Berlin, 2004.
19. F. Giazotto, J. T. Peltonen, M. Meschke, and J. P. Pekola, Superconducting quantum interference proximity transistor, *Nat. Phys.* **2010**, 6, 254-259.
20. F. Giazotto, and F. Taddei, Hybrid superconducting quantum magnetometer, *Phys. Rev. B* **2011**, 84, 215402.
21. M. Meschke, J. T. Peltonen, F. Giazotto, and J. P. Pekola, Tunnel spectroscopy of a proximity Josephson junction, *Phys. Rev. B* **2011**, 84, 214514.
22. N. W. Ashcroft, and D. N. Mermin, Solid State Physics, *Saunders College*, Philadelphia, 1976.
23. F. Giazotto, and F. Taddei, Superconductors as spin sources for spintronics, *Phys. Rev. B* **2008**, 77, 132501.
24. A. Ozaeta, P. Virtanen, F. S. Bergeret, and T. T. Heikkilä, Predicted Very Large Thermoelectric Effect in Ferromagnet-Superconductor Junctions in the Presence of a Spin-Splitting Magnetic Field, *Phys. Rev. Lett.* **2016**, 116, 097001.
25. R. Holm, and W. Meissner, Kontaktwiderstand zwischen Supraleitern und Nicht-supraleitern, *Z. Phys.* **1932**, 74, 715-735.
26. S. Kolenda, M. J. Wolf, and D. Beckmann, Observation of Thermoelectric Currents in High-Field Superconductor-Ferromagnet Tunnel Junctions, *Phys. Rev. Lett.* **2016**, 112, 057001.
27. M. A. Nielsen, and I. L. Chuang, Quantum Computation and Quantum Information, *Cambridge Univ. Press*, Cambridge, 2002.
28. S. Spilla, F. Hassler, and J. Splettstoesser, Measurement and dephasing of a flux qubit due to heat currents, *New J. Phys.* **2014**, 16, 045020.
29. N. Li, J. Ren, L. Wang, G. Zhang, P. Hänggi, and B. Li, Phononics: manipulating heat flow with electronic analogs and beyond, *Rev. Mod. Phys.* **2012**, 84, 1045-1066.
30. J. Millman, and C. C. Halkias, Electronic Devices and Circuits, *McGraw-Hill*, New York, 1967.
31. P. Horowitz, and W. Hill, The Art of Electronics, *Cambridge Univ. Press*, Cambridge, 1989.
32. F. Giazotto, P. Solinas, A. Braggio, and F. S. Bergeret, Ferromagnetic-Insulator-Based Superconducting Junctions as Sensitive electron Thermometers, *Phys. Rev. Appl.* **2015**, 4, 044016.
33. A. Ronzani, and C. Altimiras, and F. Giazotto, Highly Sensitive Superconducting Quantum-Interference Proximity Transistor *Phys. Rev. Appl.* **2014**, 2, 024005.
34. J. S. Moodera, T. S. Santos, and T. Nagahama, The phenomena of spin-filter tunnelling *J. Phys. Condens. Matter* **2007**, 19, 165202.
35. T. Tokuyasu, J. A. Sauls, and D. Rainer, Proximity effect of a ferromagnetic insulator in contact with a superconductor, *Phys. Rev. B* **1988**, 38, 8823-8833.
36. R. C. Dynes, J. P. Garno, G. B. Hertel, and T. P. Orlando, Tunneling Study of Superconductivity near the Metal-Insulator Transition, *Phys. Rev. Lett.* **1984**, 53, 2437-2440.
37. M. Tinkham, Introduction to Superconductivity, *McGraw-Hill*, New York, 1996.
38. J. Rammer, and H. Smith, Quantum field-theoretical methods in transport theory of metals, *Rev. Mod. Phys.* **1986**, 58, 323-350.
39. K. D. Usadel, Generalized Diffusion Equation for Superconducting Alloys, *Phys. Rev. Lett.* **1970**, 25, 507-509.

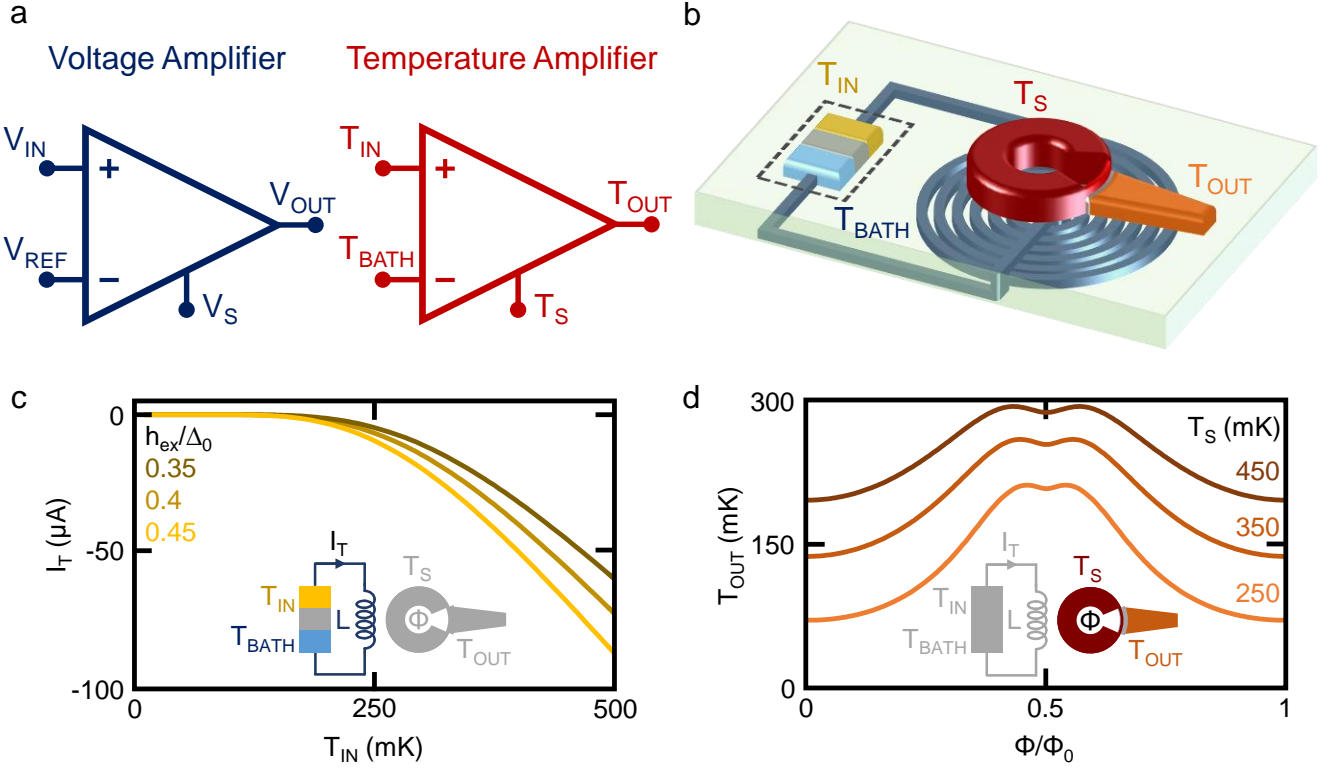


Figure 1: Phase-coherent temperature amplifier. (a) Circuit diagram symbols of voltage amplifier (blue) and temperature amplifier (red). The input (V_{IN} and T_{IN}), reference (V_{REF} and T_{BATH}) and output (V_{OUT} and T_{OUT}) signals, and the power supplies (V_S and T_S) are represented. (b) Schematic representation of the temperature amplifier: the thermoelectric element highlighted with the dashed rectangle is constituted of a metal (yellow), a ferromagnetic insulator (gray) and a superconductor (turquoise). The blue depicts the superconducting coil. The SQUIPT is composed of a S_1N_1 ring (red) and a tunnel-coupled metal probe (orange) through a thin insulator (dark gray). (c) Closed circuit thermoelectric current I_T as a function of T_{IN} for different values of h_{ex} . Parameters: $T_{BATH} = 10$ mK, $T_{CS} = 3$ K, $\Gamma = 1 \times 10^{-4}\Delta_0$, and $P = 0.95$. (d) Output temperature T_{OUT} of the SQUIPT as a function of Φ for different values of T_S . Parameters: $\Delta_{0-S_1} = 200$ μeV , $\Gamma_{S_1} = 1 \times 10^{-4}\Delta_{0-S_1}$, $l = 100$ nm, $t, w = 30$ nm, $D = 1 \times 10^{-2}$ m²/s, $\gamma = 33$, $R_T = 100$ k Ω , $\Sigma = 4 \times 10^9$ WK⁻⁶m⁻³, $V = 1 \times 10^{-20}$ m³ and $n = 6$.

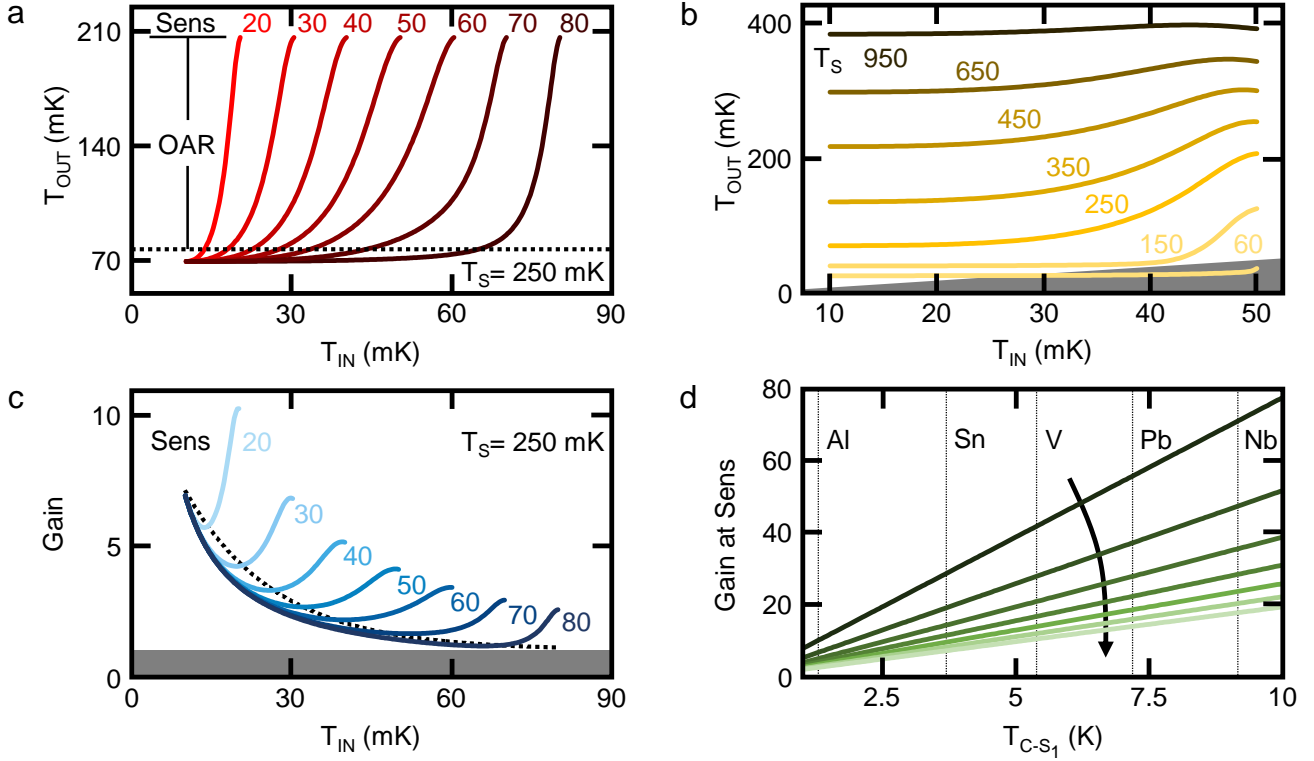


Figure 2: Thermal behavior of the phase-coherent temperature amplifier. (a) Output temperature T_{OUT} as a function of input temperature T_{IN} calculated for a supply temperature $T_S = 250$ mK and for different values of sensitivity $Sens$. The black dotted line represents the minimum value of active output $T_{OUT_{MIN}}$. The output active range OAR is shown. (b) Output temperature T_{OUT} as a function of input temperature T_{IN} calculated for a coupling L and for different values of supply temperature T_S . The gray triangle depicts the portion of the parameters space with gain $G \leq 1$. (c) Gain G as a function of input temperature T_{IN} calculated for a supply temperature $T_S = 250$ mK and for different values of sensitivity $Sens$. The gray rectangle represents the area of $G \leq 1$. The black dotted line represents the minimum value of OAR . (d) Gain G as a function of the critical temperature of the SQUIPT ring T_{C-S_1} for a constant ratio $T_{C-S_1}/T_S = 5.2$ and different values of the inductive coupling L (decreasing with the arrow direction). Cuts at critical temperatures of relevant superconducting materials are represented.

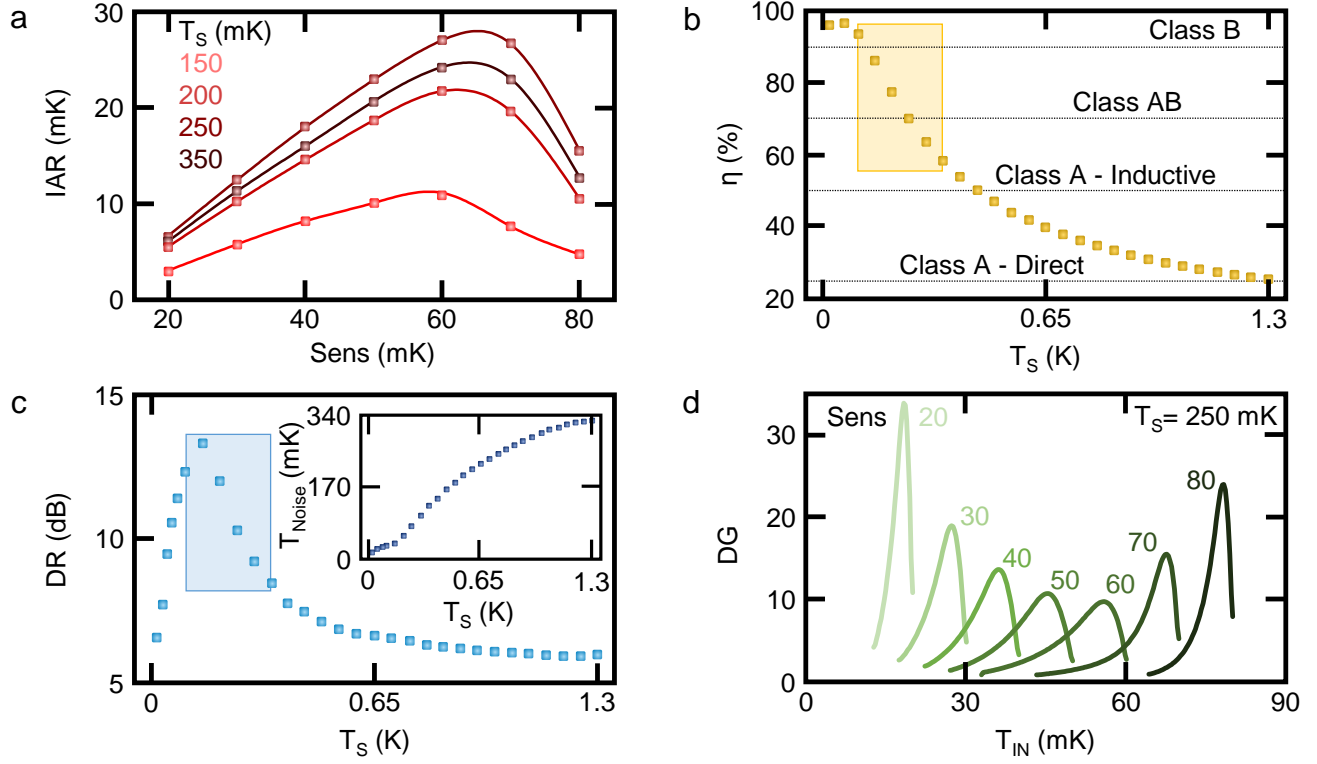


Figure 3: Figures of merit for the phase-coherent temperature amplifier. (a) Amplification range of the input temperature IAR as a function of sensitivity $Sens$ calculated for different values of the supply T_S . (b) Efficiency η as a function of the supply temperature T_S . The yellow rectangle depicts the area of maximum performances in terms of gain and active range. Typical efficiencies of common voltage amplifiers are shown for a comparison. (c) Output dynamic range DR as a function of the supply T_S . The turquoise rectangle represents the area of maximum performances in terms of G and OAR . Inset: output noise as a function of the supply temperature T_S . (d) Differential gain DG as a function of the input temperature calculated at $T_S = 250$ mK for different values of sensitivity.

Graphical TOC Entry

